

Constraints on the Inner Mass Profiles of Lensing Galaxies from Missing Odd Images

David Rusin, Chung-Pei Ma

Department of Physics and Astronomy, University of Pennsylvania, 209 S. 33rd St., Philadelphia, PA, 19104-6396

ABSTRACT

Most gravitational lens systems consist of two or four observable images. The absence of detectable odd images allows us to place a lower limit on the power-law slope of the inner mass profile of lensing galaxies. Using a sample of six two-image radio-loud lens systems and assuming a singular power-law surface density ($\Sigma \propto r^{-\beta}$) for the inner several kpc of the mass distribution, we find a statistical bound of $\beta \geq 0.94$ at 1σ and $\beta \geq 0.84$ at 2σ . Furthermore, individual mass modeling using elliptical deflectors yields $\beta \geq 0.85$ for B0739+366 and $\beta \geq 0.91$ for B1030+074. Modeling central black holes as additional point masses changes the constraints in these systems only slightly to $\beta \geq 0.84$ and $\beta \geq 0.82$, respectively. The inner mass profiles of lensing galaxies are therefore not much shallower than isothermal.

Subject headings: galaxies: structure – gravitational lensing

1. Introduction

Many properties of a galaxy can be learned from its mass profile. Measurements of galaxies' mass profiles at outer radii have provided some of the most compelling evidence for the existence of dark matter (e.g. Rubin et al. 1980). The inner mass distributions also carry a wealth of information. Depending on the type of systems under study, e.g., dwarfs, giant ellipticals, or clusters, quantities such as the slope of the radial profile, ellipticity, and core radius can offer valuable insight into the stellar content, formation history, or the nature of dark matter in these systems.

Strong gravitational lensing is an excellent tool for studying the inner several kpc of galaxies at intermediate redshift ($z \sim 0.5$). Lensing has already taught us much about the inner mass distribution of elliptical galaxy lenses by essentially ruling out constant mass-to-light ratio models, based on poor fits to individual lens systems (Kochanek 1995; Grogin & Narayan 1996; Romanowsky & Kochanek 1999) and an inability to reproduce observed image separations (Maoz & Rix 1993). Power-law mass profiles with surface mass density $\Sigma(r) \propto r^{-\beta}$, and the isothermal case ($\beta = 1$) in particular, provide improved models of lensing mass distributions while remaining statistically consistent. Mass modeling for only a few systems has thus far yielded direct constraints on the power-law profile: QSO 0957+561 ($0.82 \leq \beta \leq 0.93$; Grogin & Narayan 1996), MG1131+0456

($1.2 \leq \beta \leq 1.6$; Chen et al. 1995), B1608+656 ($0.8 \leq \beta \leq 1.2$; Koopmans & Fassnacht 1999), MG 1654+1346 ($0.9 \leq \beta \leq 1.1$; Kochanek 1995), and B1933+503 ($0.7 \leq \beta \leq 1.0$; Cohn et al. 2000). Unfortunately, most two-image lenses do not provide a sufficient number of constraints to allow for a detailed investigation of the galaxy mass profile.

In this letter we explore a method for constraining the slope of the inner mass profile of lensing galaxies in two-image systems. This technique takes advantage of the lensing property that as the mass profile is made shallower (relative to isothermal), a faint image close to the center of the lens becomes more prominent (Narasimha et al. 1986; Blandford & Kochanek 1987). One can compute the frequencies at which detectable three-image systems are produced as a function of the power-law index and axis ratio of the mass distribution (§ 2). The absence of observed third images therefore allows us to constrain the steepness of the lens mass profile. To achieve this goal we employ two complementary approaches. First (in § 3), we derive a lower statistical limit on the characteristic slope of the inner mass profile of lensing galaxies by performing a likelihood analysis on a sample of six radio-loud two-image lens systems. Second (in § 4), we use mass modeling to constrain the profiles of two individual lensing galaxies, B0739+366 (Marlow et al. 2000) and B1030+074 (Xanthopoulos et al. 1998). The effect of central black holes is also explored.

2. Frequency of Detectable Triple Systems

The inner mass profile of lensing galaxies is approximated as a singular power-law ellipsoid (SPLE; e.g. Barkana 1998), with projected surface mass density

$$\Sigma(x_1, x_2) \propto [x_1^2 + f^2 x_2^2]^{-\beta/2},$$

where β is radial profile and f is the axial ratio. For the isothermal case, $\beta = 1$. The SPLE likely oversimplifies the overall mass distribution in galaxies but is a reasonable model for the inner several kpc that is probed by strong lensing.

We focus on the three-image systems produced by lenses with the SPLE mass density.¹ The imaging properties of the SPLE depend sensitively on the slope of the mass profile (e.g. Blandford & Kochanek 1987). Of primary importance for singular mass distributions is that the radial critical curve exists only if the profile is shallower than isothermal ($\beta < 1$). In this regime, an odd number of lensed images with nonzero magnification is created. For $\beta \sim 1$, the positive parity image within the radial critical curve is highly demagnified and could easily escape detection. As the profile becomes shallower, the radial critical curve grows and the radial caustic shrinks in size (Fig. 1), and the magnification of the central image increases. For small enough f , the cusps of the tangential caustic become exposed (Fig. 1b), leading to the production of naked cusp configurations. A source

¹The additional fifth image for quads tends to be significantly more demagnified than the corresponding third image for doubles (Wallington & Narayan 1993). Therefore the absence of a fifth image in quads leads to much poorer constraints on the mass profile.

in the naked cusp region will produce three images on the same side of the lens with large and similar magnifications (e.g. Kormann et al. 1994). We will refer to these naked cusp systems as “Type II” and all other three-image systems as “Type I.” Near-isothermal models with reasonable axial ratios ($f \geq 0.4$) produce predominately Type I systems.

In order to make use of the information provided by unobserved odd images, one must first determine the frequency at which observable three-image systems are produced by power-law deflectors. To this end, we have performed Monte Carlo simulations in which sources are placed randomly in the Type I and Type II caustic regions of the SPLE for various combinations of β (≤ 1) and f . In each trial the lens equation is numerically inverted using a modified downhill simplex technique (Press et al. 1992) to solve for all images. The magnification ratio of the brightest to faintest image (μ_1/μ_3) is then tabulated. All calculations make use of the rapidly converging series solutions for the deflection angles and magnification matrices of power-law mass distributions derived by Barkana (1998) and implemented in the “FASTELL” software package. We illustrate in Fig. 2 the fraction of three-image systems that have flux ratios $\mu_1/\mu_3 \leq 100$ as a function of β and f . The value of 100 is used here because as discussed in the next section, the sensitivity of radio follow-up observations should guarantee the detection of any faint third image whose flux is within a factor of 100 of the brightest image. The dependence on β of the curves in Fig. 2 can be understood as follows. For $\beta = 1$, the radial critical curve degenerates into a point and the third image is infinitely demagnified, so $\mu_1/\mu_3 \rightarrow \infty$, and the fraction of Type I configurations is zero. As the profile becomes shallower than isothermal, the radial critical curve grows in size, the third image inside the radial critical curve becomes brighter, and P_I increases initially as β decreases from 1 (Fig. 2a). As β is decreased further, however, Fig. 2a shows that the Type I fraction begins to decline beyond a cutoff that depends on the axial ratio f . For β below this cutoff, Type II systems begin to dominate (Fig. 1 and Fig. 2b), and a large fraction of three-image systems should appear as three relatively bright images on the same side of the lens, which has never been observed. A profile much shallower than isothermal is therefore highly disfavored, as observable three-image systems become the majority for $\beta \leq 0.6$ (Fig. 2c).

We note that whenever a Type II system is produced, the magnifications of the three images are similar enough so that the detectability condition of $\mu_1/\mu_3 \leq 100$ is almost always satisfied. This implies that for a given β and f , one can compute the Type II fraction P_{II} in Fig. 2b by simply dividing the area of the Type II region in the source plane shown in Fig. 1 by the sum of Type I and II areas. We have verified that results from this method indeed agree with the full Monte Carlo calculations.

3. Statistical Constraints on Mass Profiles from Radio Data

Radio-loud gravitational lens systems are ideal targets with which to search for faint odd images. Such systems can be investigated with high dynamic range maps that are not contaminated by galaxy emission, which might otherwise mask the presence of faint additional images close to the

center of the lens. The most extensive radio lens search is the combined Jodrell-VLA Astrometric Survey (JVAS; Patnaik et al. 1992; Browne et al. 1998; Wilkinson et al. 1998; King et al. 1999) and Cosmic Lens All-Sky Survey (CLASS; Browne et al. 1999; Myers et al., in preparation). Lens candidates are selected from snapshot imaging with the Very Large Array (VLA) and followed up with deep observations using the Multi-Element Radio Linked Interferometer Network (MERLIN) and the Very Long Baseline Array (VLBA), each of which offer excellent sensitivity (RMS = 0.04 – 0.05 mJy/beam). The compact nature of the sources selected by CLASS should allow the detection of even very faint additional lensed components. Since typical CLASS lens systems have a primary component with $S_1 \geq 20$ mJy at 5 GHz, a conservative 5σ limit should ensure the detection of any faint third image such that the magnification ratio is $\mu_1/\mu_3 \leq 100$. A number of radio lens systems are significantly brighter than 20 mJy, and in such cases demagnified additional components would be more readily detectable.

The combined JVAS/CLASS lens survey currently contains seven two-image gravitational lens systems. We remove B1127+365 (Koopmans et al. 1999) due to its compound deflector, and take the remaining six lenses as our sample. Each of the systems has been investigated with deep MERLIN and VLBA observations, and no additional images have been found down to the 5σ detection limit (~ 0.225 mJy) of the maps. For each lens system, Table 1 lists the flux density of the brightest image in the most sensitive map and the corresponding constraint on the magnification ratio ($r = S_1/0.225$ mJy).

The frequency $p(\beta, f, r_i)$ at which detectable three-image lens systems with $\mu_1/\mu_3 \leq r$ are produced by a given deflector model can be calculated as a function of β and f , as demonstrated in Fig. 2. The probability that a particular lens system will be observed as a double rather than a triple is therefore $1 - p(\beta, f, r_i)$. To evaluate the consistency of a given mass model with the lack of observed third images, we calculate the likelihood $L(\beta, f) = \prod_{i=1}^6 [1 - p(\beta, f, r_i)]$ and plot the results in Fig. 3 as a function of β for various values of the mass axial ratio f . The likelihood function does not need to be normalized, as the isothermal slope (or steeper) automatically provides a preferred fit of $L = 1$ (i.e., it allows the formation of no Type I systems). Because flatter deflectors produce a greater fraction of three-image systems (see Figs. 2a and 2c), the spherical case offers the broadest constraint. We find that $\beta \geq 0.94$ at 1σ , $\beta \geq 0.88$ at 90%, and $\beta \geq 0.84$ at 2σ for a spherical power-law deflector. (Even overly conservative detection limits of $r = 100$ for each lens system would still require rather steep profiles with a 2σ bound of $\beta \geq 0.75$.) Flattened mass distributions yield tighter constraints. If we assume a representative axial ratio of $f \sim 0.5$, for example, $\beta \geq 0.88$ at 2σ .

4. Mass Modeling of Two Lens Systems

To test how our statistical constraint compares with those from the mass modeling of individual lens systems, we now attempt to directly constrain the profiles of specific galaxies. For simplicity we will only consider two-image systems lensed by an isolated elliptical galaxy whose centroid relative

to the lensed images is well determined, i.e., B0739+366 (Marlow et al. 2000) and B1030+074 (Xanthopoulos et al. 1998).

Modeling of these two systems is performed with data available in the literature. The position of the lens galaxy is fixed according to the respective optical imaging. In each trial we set the power-law index β to some test value and optimize the remaining five free model parameters: the galaxy normalization, axial ratio, position angle, and the source coordinates. Since the radio data provide five constraints (coordinates of the two images and a flux density ratio), the best-fit model can reproduce the image properties perfectly. At the end of each trial the recovered source position is numerically inverted to solve for all images. The magnification of the third (unseen) image relative to the brightest image is then compared to current detection limits, as listed in Table 1. The predicted ratios μ_1/μ_3 as a function of mass profile are plotted in Fig. 4. The lack of detectable third images implies that $\beta \geq 0.85$ for B0739+366 and $\beta \geq 0.91$ for B1030+074.

There is significant evidence that black holes exist at the center of elliptical galaxies. Mao et al. (2000) recently demonstrate that if lensing galaxies are modeled as an isothermal ellipsoid with a finite core radius, the addition of a central black hole can steepen the inner profile and suppress the magnification of the third image. In our analysis we have instead used a singular ellipsoid with an arbitrary power index β to approximate the inner mass distribution from all forms of matter. Our constraints thus far are therefore on the total contributions from baryons, dark matter, and perhaps black holes. However, to quantify the separate contribution from potential black holes, we also model these two lenses by adding a central point mass to the singular ellipsoid according to the empirical relation $M_{BH} \sim 1.3 \times 10^8 M_\odot (\sigma_v/200 \text{ km s}^{-1})^{4.72}$ between black hole mass and velocity dispersion (Merritt & Ferrarese 2000), which combines the measurements of Ferrarese & Merritt (2000) and Gebhardt et al. (2000). To obtain the black hole mass we use the isothermal velocity dispersion required to produce the observed image separation (which should be a good approximation so long as we are investigating mass profiles close to isothermal), and find $M_{BH} \sim 1.7 \times 10^7 M_\odot$ for B0739+366 and $M_{BH} \sim 3.7 \times 10^8 M_\odot$ for B1030+074. Including a central black hole introduces some cosmological dependence on the mass model, so we choose a flat $\Omega_m = 0.3$ universe with $H_o = 65 \text{ km s}^{-1} \text{ Mpc}^{-1}$. The resulting magnification ratio curves for each lens are plotted in Fig. 4. We find that when central black holes are modeled separately as point masses, the constraints become $\beta \geq 0.84$ for B0739+366 and $\beta \geq 0.82$ for B1030+074, a less than 10% change from the pure SPLE case. Using the shallower $M_{BH} - \sigma_v$ relation from Gebhardt et al. 2000 we find $\beta \geq 0.82$ for B0739+366 and $\beta \geq 0.84$ for B1030+074. Note that the slightly weaker profile constraints in models with a black hole are largely due to the complete demagnification of the central image for steeper profiles (Fig. 4), an effect similar to that described in Mao et al. 2000.

5. Discussion

Using the detection limits for faint third images in six radio-loud doubly-lensed systems from JVAS and CLASS, and assuming a singular power-law surface mass density ($\Sigma \propto r^{-\beta}$), we have

obtained a lower bound on the power-law index β for the inner mass profiles of typical lensing galaxies. The lack of detectable third images implies a statistical bound of $\beta \geq 0.94$ at 1σ and $\beta \geq 0.84$ at 2σ (for spherical deflectors). This constraint argues that the total mass in the form of baryons, dark matter, and perhaps black holes at the inner parts of lensing galaxies follows a profile that is not much shallower than isothermal.

We have also used mass modeling and the lack of a detectable third image to constrain the individual profiles of two lensing galaxies that have well determined centroids. We find $\beta \geq 0.85$ for B0739+366 and $\beta \geq 0.91$ for B1030+074 when a singular ellipsoid is used to approximate the lensing galaxy. If the lensing galaxy is assumed to harbor a central black hole which is modeled separately as a point mass, we find only slightly different bounds of $\beta \geq 0.84$ for B0739+366 and $\beta \geq 0.82$ for B1030+074. We note that adding core radii of any size to our mass distributions would only increase the prominence of faint central images, thereby tightening constraints. Because elliptical deflectors produce a higher frequency of three-image lens systems (Fig. 2c), it is likely that the effects of more complex mass distributions tend to offset one another, so that the statistical lower bound on the mass profile derived using spherical deflectors is within a few percent of reality.

Although limits on the profile slope would certainly be improved by increasing the number of radio lens systems in the analysis, little improvement is expected by obtaining deeper maps of existing lenses. Our Monte Carlo simulations demonstrate that detectable three-image systems with small μ_1/μ_3 are much more common than those with large μ_1/μ_3 . As a result, deeper observations quickly lead to diminishing returns for the statistical profile constraints. In addition, near-isothermal profiles ($0.95 \leq \beta < 1$) produce extremely faint third images that would be virtually impossible to detect with any instrument.

In summary, the lack of detectable odd images rules out a large region of shallow profiles for the inner several kpc of galaxy mass distributions, and therefore provides corroborating evidence for the popular isothermal model favored by stellar dynamics (Rix et al. 1997), studies of elliptical galaxies with X-ray halos (Fabbiano 1989) and previous constraints from gravitational lensing. We stress that our result applies only to the total profile, as lensing cannot distinguish between the individual mass constituents. Compared with the universal dark matter profiles of $\beta \lesssim 0.5$ reported in various numerical simulations (e.g. Navarro et al. 1997; Moore et al. 1999), the near or steeper than isothermal slope favored by lensing studies indicates that either the centers of elliptical galaxies are dominated by baryonic components comprised of stars and possibly black holes, or that the dark matter has a profile steeper than in N -body simulations.

This paper would not have been possible without the hard work of everyone in the JVAS/CLASS team. We thank Paul Schechter for interesting discussions. D. R. acknowledges support from the Zaccheus Daniel Foundation. C.-P. M. acknowledges support of an Alfred P. Sloan Foundation Fellowship, a Cottrell Scholars Award from the Research Corporation, a Penn Research Foundation Award, and NSF grant AST 9973461.

REFERENCES

- Barkana, R. 1998, *ApJ*, 502, 531
- Biggs, A.D., Browne, I.W.A., Helbig, P., Koopmans, L.V.E., Wilkinson, P.N., Perley, R.A. 1999, *MNRAS*, 304, 349
- Blandford, R.D., Kochanek, C.S. 1987, *ApJ*, 321, 658
- Browne, I.W.A., Wilkinson, P.N., Patnaik, A.R., Wrobel, J.M. 1998, *MNRAS*, 293, 257
- Browne, I.W.A., et al. 1999, to appear in “Gravitational Lensing: Recent Progress and Future Goals”, eds. T. Brainerd and C. Kochanek
- Chen, G.H., Kochanek, C.S., Hewitt, J.N. 1995, *ApJ*, 447, 62
- Cohn, J.D., Kochanek, C.S., McLeod, B.A., Keeton, C. R. 2000, *ApJ*, submitted (astro-ph/0008390)
- Fabbiano, G. 1989, *AR&A*, 27, 87
- Ferrarese, L., Merritt, D. 2000, *ApJ*, 539, L9
- Gebhardt, K. et al. 2000, *ApJ*, 539, L13
- Grogin, N.A., Narayan, R. 1996, *ApJ*, 464, 92
- King, L.J., Browne, I.W.A., Marlow, D.R., Patnaik, A.R., Wilkinson, P.N. 1999, *MNRAS*, 307, 225
- Kochanek, C.S. 1995, *ApJ*, 445, 559
- Koopmans, L.V.E., de Bruyn, A.G., Jackson, N.J. 1998, *MNRAS*, 295, 534
- Koopmans, L.V.E., et al. 1999, *MNRAS*, 303, 727
- Koopmans, L.V.E., Fassnacht, C.D. 1999, 527, 513
- Kormann, R., Schneider, P., Bartelmann, M. 1994, *A&A*, 284, 285
- Mao, S., Witt, H.J., Koopmans, L.V.E. 2000, *MNRAS*, submitted (astro-ph/0007011)
- Maoz, D., Rix, H.-W. 1993, *ApJ*, 416, 425
- Marlow, D.R., et al. 2000, *AJ*, submitted (astro-ph/0008037)
- Merritt, D., Ferrarese, L. 2000, *ApJ*, in press (astro-ph/0008310)
- Moore, B., Quinn, T., Governato, F., Stadel, J., Lake, G. 1999, *MNRAS*, 310, 1147
- Myers, S.T., et al. 1999, *AJ*, 117, 2565
- Narasimha, D., Subramanian, K., Chitre, S.M. 1986, *Nature*, 321, 45
- Navarro, J. F., Frenk, C. S., White, S. D. M. 1997, *ApJ*, 490, 493
- Patnaik, A.R., Browne, I.W.A., Wilkinson, P.N., Wrobel, J.M. 1992, *MNRAS*, 254, 655
- Press, W.H., Teukolsky, S.A., Vetterling, W.T., Flannery, B.P. 1992, “Numerical Recipes in C,” Cambridge University Press
- Rix, H.-W., de Zeeuw, P.T., Cretton, N., van der Marel, R.P., Carollo, C.M. 1997, *ApJ*, 488, 702

Romanowsky, A.J., Kochanek, C.S. 1999, ApJ, 516, 18

Rubin, V.C., Thonnard, N., Ford, W.K. 1980, ApJ, 238, 471

Wallington, S., Narayan, R. 1993, ApJ, 403, 517

Wilkinson, P.N., Browne, I.W., Patnaik, A.R., Wrobel, J.M., Sorathia, B. 1998, MNRAS, 300, 790

Xanthopoulos, E. et al. 1998, MNRAS, 300, 649

| Lens | Instrument/Frequency | S_1 (mJy) | r | Reference |
|-----------|----------------------|-------------|------|------------------------------|
| B0218+357 | VLBI 5 GHz | 515 | 2285 | Biggs et al. 1999 |
| B0739+366 | MERLIN 5 GHz | 35 | 155 | Marlow et al. 2000 |
| B1030+074 | MERLIN 5 GHz | 325 | 1445 | Xanthopoulos et al. 1998 |
| B1152+199 | MERLIN 5 GHz | 48 | 215 | Myers et al. 1999 |
| B1600+434 | MERLIN 5 GHz | 45 | 200 | Koopmans et al. 1998 |
| B2319+051 | MERLIN 5 GHz | 47 | 210 | Rusin et al., in preparation |

Table 1: The radio lens sample. Flux densities for the brightest images are from the highest dynamic range maps available for each lens. If this image contains multiple subcomponents, S_1 is the sum of the subcomponent flux densities. Some values used in this analysis are not directly quoted in papers currently in the literature, but are taken from the CLASS data archive or from papers in preparation. The magnification ratio detection limit r is defined as $S_1/0.225$ mJy. While the values of r for B0218+357 and B1030+074 appear almost unreasonably large, setting each to $r = 1000$ decreases the 2σ statistical constraint on β by only 0.01.

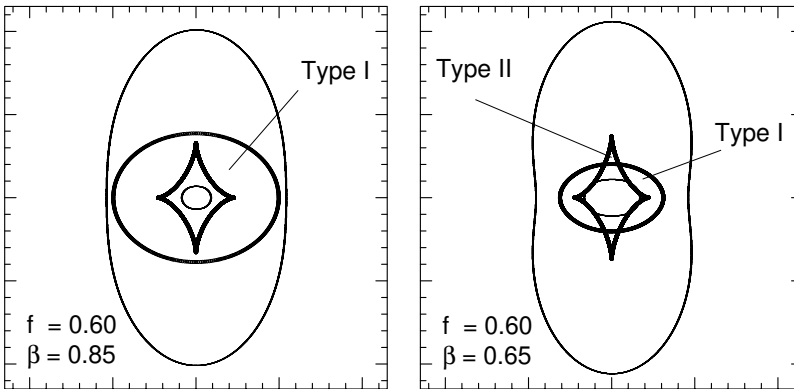


Fig. 1.— Lensing properties of the SPLE (shown: $f = 0.6$). Caustics (dark lines) separate different imaging regions. The critical curves are drawn with thin lines. Left: $\beta = 0.85$. Right: $\beta = 0.65$. Note how decreasing β increases the size of the radial (inner) critical curve while decreasing the size of the radial (outer) caustic. This leads to a larger fraction of detectable three-image configurations.

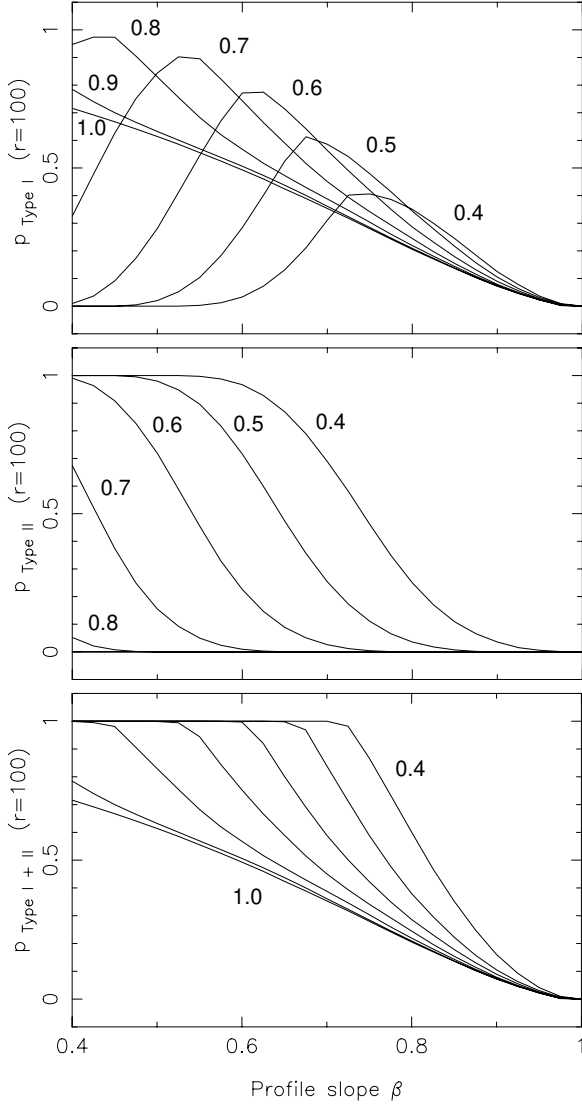


Fig. 2.— Frequency of producing observable three-image configurations with $\mu_1/\mu_3 \leq 100$, as a function of profile slope β . Different axial ratios (f) are marked. (a) Top: Type I systems. (b) Middle: Type II systems. (c) Bottom: Type I + II systems.

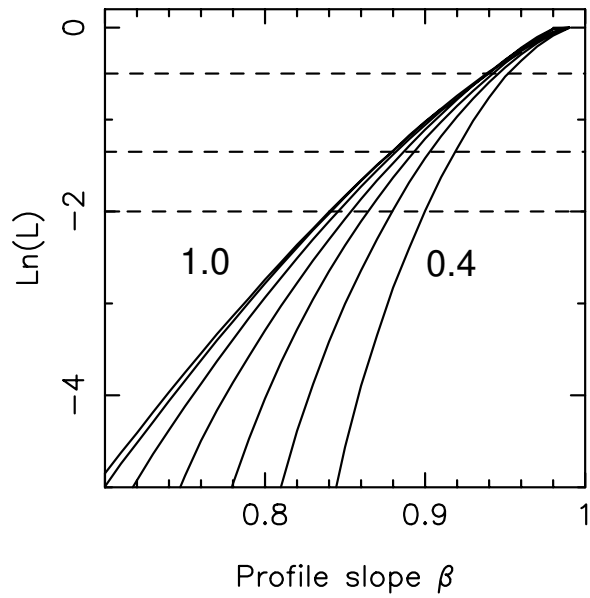


Fig. 3.— Statistical constraints on the profile slope. Likelihood plot for three-image lens systems to be detected as doubles. Various values of the axial ratio f are shown: $f=1.0, 0.9, \dots, 0.4$ (left to right). The gaussian 1σ , 90% and 2σ confidence limits are marked.

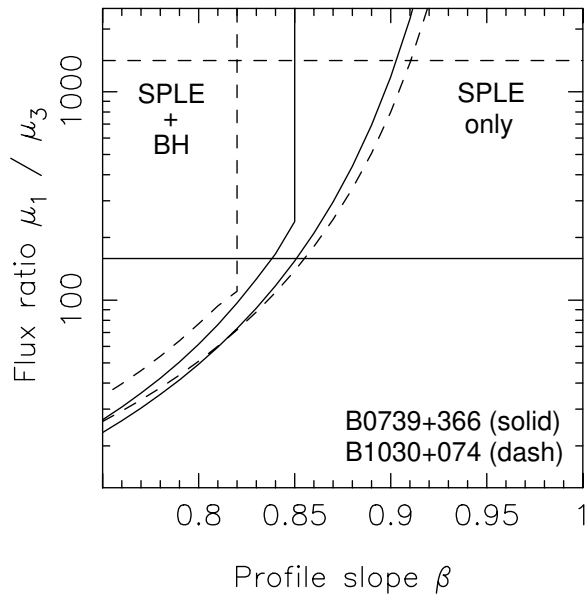


Fig. 4.— Flux ratio μ_1/μ_3 as a function of β from the mass modeling of B0739+366 (solid lines) and B1030+074 (dash lines). Leftmost curves denote models that include a central black hole, according to the relation of Merritt & Ferrarese 2000. Rightmost curves are for a pure SPLE. Note that a black hole destroys the third image for $\beta \geq 0.85$ in B0739+366 and $\beta \geq 0.82$ in B1030+074. The respective detection limits for third images are marked as horizontal lines and determine the profile constraints.